High-Gain Millimeter-Wave Antenna-in-Display Using Non-Optical Space for 5G Smartphones

Jeongtaek Oh, *Graduate Student Member, IEEE*, Byeongjin Kim, *Graduate Student Member, IEEE*, Sangrock Yoon, *Member, IEEE*, Kiseo Kim, Eun Jin Sung, *Member, IEEE*, and Jungsuek Oh, *Senior Member, IEEE*

Abstract—This article presents a high-gain display-integrated antenna topology, for the first time, embedding radiating traces into a nonoptical space, referred to as the dead space (DS), which is the edge part of the display panel; however, it does not perturb the optical illumination of the display. Thus, the proposed antenna topology is denoted as antenna-in-display (AiD). To fit the extremely narrow embedding conditions of the given DS ($=0.03 \lambda_0$ at 28 GHz), a new-shape coplanar waveguide (CPW)-fed folded dipole antenna was devised and efficiently tailored in the DS area. The bottom side of the panel was modified to render the effect of a coplanar defected ground structure (CDGS) for antenna minimization, and a new asymmetrical antenna geometry was proposed for wideband impedance matching and broadside radiation pattern. Compared with conventional studies, the proposed antenna concept provides an improved gain resulting from the good conductive metal in DS, the complete display visibility, and touch sensor compatibility, whereas the previous antenna-on-display (AoD) approaches inherently suffer from the limited gain obtained at the expense of lower conductivity of the optically invisible antenna electrodes. Because the proposed AiD concept enables the direct fabrication of antenna traces into the DS area of the display panel, eliminating need for an additional film, a lower package profile, and cost reduction can be achieved. The proposed prototype was fabricated and verified using an actual smartphone. The measured data confirm 12.32 dBi gain, 54.3% radiation efficiency, and 3 dB gain bandwidth larger than 3 at 28 GHz.

Index Terms—5G smartphone, antenna-in-display (AiD), millimeter-wave (mm-Wave) antenna.

I. INTRODUCTION

ACCORDING to the latest 3GPP standard, operating bands of millimeter-wave (mm-Wave) 5G communication cover high-frequency bands such as 24.25–29.5 GHz (n257, n258, and n261), 37–43.5 GHz (n259 and n260), and 47.2–48.2 GHz (n262) [1]. Because of their unprecedented high frequency, mmWave 5G antenna modules are required to have high radiation efficiency and wide beam coverage to overcome severe path loss when they are implemented in cellular devices. Antenna-on-chip (AoC), antenna-in-package (AiP), and antenna-on-package (AoP) technologies have been frequently studied as prominent solutions for the millimeter-wave antennas to be implemented in cellular devices [2], [3], [4], [5], [6], [7], [8], [9], [10], [11], [12], [13], [14], [15], [45], [46], [47]. However, AoC, AiP, and AoP solutions are now being challenged by the decreased integration and packaging area because the bezel area where antennas are merged with the cellular devices is gradually disappearing due to the global trend of wide display and new display form factors such as rollable or foldable displays. To determine an integration-scenario acceptable breakthrough, the idea of using a display region as a part of the antenna real estate has emerged in recent years [16], [17], [18], [19], [20], [21], [22], [23], [24], [44].

Most display antennas are implemented by fabricating the antenna on a distinct transparent film and mounting it on the uppermost cover window or inserting it between the cover window and metallic display panel, such as organic light-emitting diodes (OLEDs) or liquid crystal displays (LCDs) [16], [17], [18], [19], [20], [21], [22], [23]. In this case, the conductive display panel functions as a ground plane for the antenna. Therefore, the antenna electrode for a patch-type antenna must be separated by at least several hundred micrometers from the display panel, in general, which ensures a moderate level of radiation efficiency and impedance bandwidth by securing a sufficient thickness of the substrate. Moreover, the antenna electrode must be designed in a transparent or invisible form for display visibility, as it is placed on the display. Most antenna electrodes are made up of mesh-grid metal or transparent metal [e.g., indium–tin oxide (ITO)] [25], [26], [27], [28], [29], [30], [31], [44]. Another option for the display antenna concept was proposed and verified analytically [24], where a slot in the modified RGB color pixel in the active matrix OLED (AMOLED) panel is a part of the antenna structure. However, the operating frequency band of the antenna must be 60 GHz or higher due to the micrometer size of the RGB color pixels, making it inappropriate for millimeter-wave 5G frequencies.

Despite their fascinating industrial potential, current display antennas face critical issues. First, issue is the necessity of a distinct total thickness of the display and cellular device,

which is resulted from the additional fabrication of the film and assembly with the display. Second, conventional display antennas inherently have low radiation efficiency due to the low conductivity of the transparent metal and the high sheet resistance of the mesh-grid metal sheet. Third, the electrodes of the conventional display antenna disturb the touch sensor layer on the display panel, exacerbating the touch sensitivity. Finally, display antennas integrated on the cover window of the display are vulnerable to physical or environmental damage because they are located at the outermost side of the cellular devices.

In this study, we propose a novel display antenna concept that incorporates the integration of the antenna electrode into the narrow nonoptical space, "dead space (DS)," in a display panel in which small area can be exposed to the mmWave radiation but separated from the active area (AA). In this sense, the proposed antenna is denoted as antenna-in-display (AiD), and we achieved a breakthrough with the aforementioned inherent difficulties in the conventional display antennas. To verify this concept, we fabricated an antenna on a cyclo-olefin polymer (COP) film using photolithography and integrated it with the DS of the display panel by inserting a very thin optically clear adhesive (OCA) to realize the concept as closely as possible. Section II presents and analyzes the antenna design and space it exists. The asymmetric structure of the proposed coplanar waveguide (CPW)-fed folded dipole antenna and the coplanar defected ground structure (CDGS) of CPW were evaluated. In Section III, the simulation and measurement results of the display-integrated AiD are discussed and compared with those of conventional display antennas.

II. ANTENNA DESIGN

The novel concept of the AiD is described in an exploded view of a smartphone, with strict definitions of the DS, the AA, and the bezel area in Fig. 1. The DS, where the proposed antenna is designed, refers to the nonoptical space between the edge of the dielectric layer and the metal layer in the display panel, as shown in Fig. 1. Here, the DS is tightly determined as $0.03 \lambda_0$, which is near-adjacent from metallic components, including numerous biasing lines, such as pixel and transistor biases. In previous research, the DS was either assumed to be a probing area for the transmission line [18] or it was simply ignored because of the short length of $0.09 \lambda_0$, where λ_0 is the free-space wavelength at 28 GHz [16], [17], [18], [19], [20], [21], [22], [23]. We first demonstrate that it is possible to realize the 28 GHz antenna only on the DS that is structurally distinguished from AA under the actual integration conditions of a 5G smartphone. The proposed antenna is completely invisible to the user. In addition, the disturbance of the touch sensor function in the display area can be minimized, as discussed in Section III. Furthermore, the antenna can be made up of solid and highly conductive metal, enabling high antenna gain, whereas conventional display antennas consisted of resistive mesh-grid metal or low-conductivity transparent metal (e.g., ITO) suffering from low gain.

If the antenna is directly printed on the DS of the display panel through a single fabrication process, the flexible polyimide (PI) film of the panel will be extended and employed
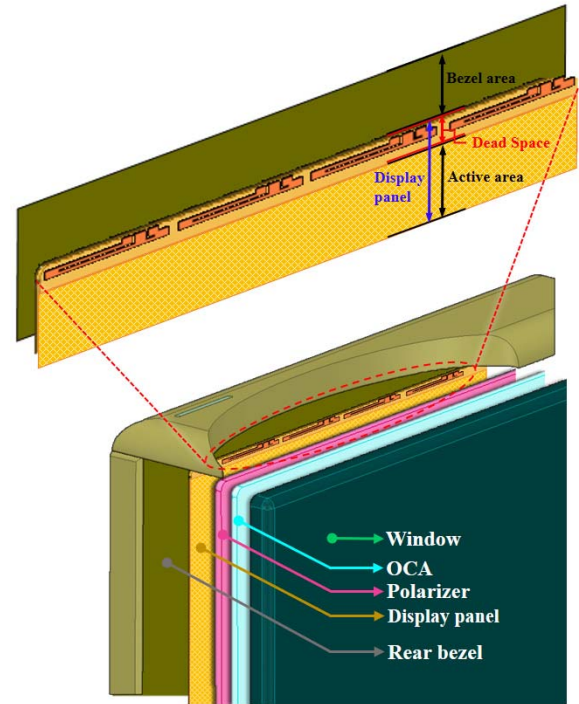

Fig. 1. Illustration of AiD concept for smartphone.

as a substrate for the CPW. There are some useful legacies of antennas based on flexible PI films [31], [32] and small-size wideband antenna design techniques [33], [34], [35], [36], [37], [38], [39], [40]. From an economic perspective, if the proposed AiP configuration is applied for mass production, the integration cost can be significantly reduced because the prior additional steps of fabricating the separate antenna-film layer and assembling it on the display panel can be removed. Modifying the entire fabrication process of the display panel to integrate the proposed antenna directly into the actual DS region of the display panel is too complicated and expensive to be considered in the prototype testing stage. We designed our antenna sample layer to be as close as possible to the display panel layer, which can be considered as the same-layer integration electromagnetically. The CPW-fed asymmetric folded dipole antenna is fabricated on a COP film with a thickness of 5000 Å, turned upside down, and affixed to the display panel by a super-thin OCA film (25 μm) so that the antenna is located as close as possible to the DS of the display panel.

The length of the antenna must be less than $0.03 \lambda_0$ for an actual narrow space of the DS. Therefore, the complexity in designing the proposed antenna between the metal layer of the display panel and the ground of the CPW had to be addressed with fixed length dimensions. The crucial design parameters are explained in detail.

A. CDGS of CPW

In the first design step, the left side of Fig. 2(b) shows a symmetric slot antenna in the DS without a separation of the CPW ground from the antenna. The design parameters of this antenna are the width of the slot (W_s) and the width of the
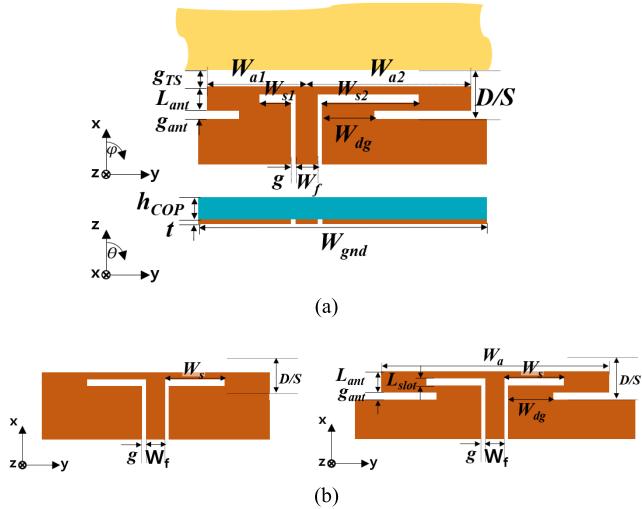
Fig. 2.   Antenna geometries: (a) proposed antenna of asymmetric folded dipole and (b) symmetric slot antenna without CDGS (left) and asymmetric slot antenna with CDGS (right).
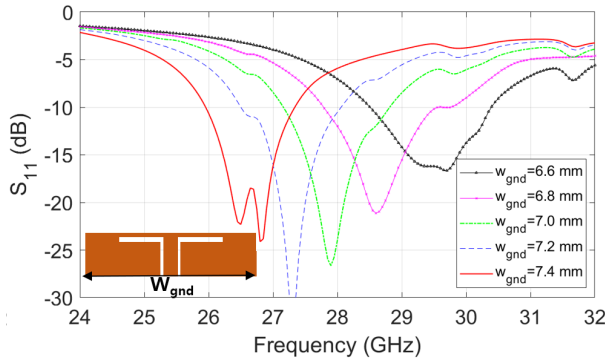

Fig. 3.   Simulated reflection coefficient: effect of design parameter (W_{gnd}) of symmetric antenna (see Fig. 2(b), left).

CPW ground (W_{gnd}). The antenna width parameter (W_{ant}) is physically the same as the width of the CPW ground (W_{gnd}), which determines the resonant frequency, as shown in Fig. 3. In the next step, the CDGS is applied by defecting the CPW ground surrounding the slots of the antenna. The CDGS separates the antenna width parameter (W_{ant}) from the CPW ground width parameter (W_{gnd}), with a new ground factor W_{dg}. The resonant frequency is determined by the antenna width (W_{ant}), whereas it is independent of the change of the ground width (W_{gnd}), as shown in Fig. 2(b). It is heuristically demonstrated that the overall width can be minimized by $0.49\lambda_0$ at 28 GHz, which is shorter than $0.65\lambda_0$ width of the antenna without a CDGS. This suggests that employing the proposed CDGS can achieve minimization of the antenna width, even under the narrow DS condition of the smartphone display panel. This allows for narrowing the interelement spacing for the phased-array configuration of the proposed antenna to suppress undesired grating lobes and decrease the sidelobe level. For the additional effect, Fig. 4 shows that the resonant frequency of the proposed antenna with the CDGS is less dependent on W_{gnd} than that of the antenna without
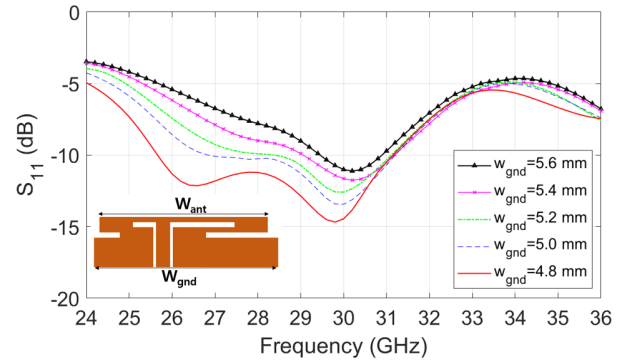

Fig. 4.   Simulated reflection coefficient: effect of design parameter (W_{gnd}) of the proposed antenna [see Fig. 2(a)].
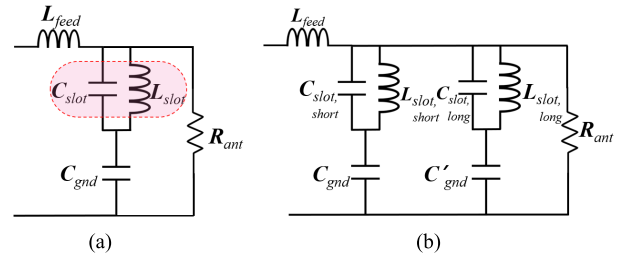

Fig. 5.   Equivalent circuit for the CPW-fed inductive slot antenna: (a) symmetric case and (b) asymmetric case.

the CDGS. Instead, impedance matching and bandwidth can be improved by varying the dimension of W_{gnd}.

B. Asymmetrically Folded Dipole Antenna

This section describes and validates the effectiveness of the asymmetric folded dipole topology of the proposed antenna, enabling a broader bandwidth and near-broadside radiation.

Fig. 5(a) shows the equivalent circuit for the symmetrical antenna in Fig. 2(b), which is slightly different from the equivalent circuit in [34]. The short-circuited slots on both sides from the middle of the signal line can be modeled as identical parallel LC resonators, sharing the same resonant frequency. However, the equivalent circuit for the asymmetrical antenna in Fig. 2(a) is different as shown in Fig. 5(b) because the slots on the left and right sides from the middle of signal line have different widths along the y-direction. The two distinct parallel LC resonators in the equivalent circuit result in two separate resonant frequencies. Therefore, the antenna can be designed to have two close resonant frequencies, thereby broadening the impedance bandwidth. Figs. 6–8 show the dependence of resonant frequencies on the widths of slots. Fig. 6 shows the first step of impedance matching in higher operating bandwidth by the change in the shorter width of slot (W_{s1}) when the value of W_{s2} is fixed. For the next step, Fig. 7 shows the impedance matching of the lower resonant frequency by the change in the longer width of the slot (W_{s2}) when the value of W_{s1} is fixed. The way of optimizing procedure is described in the following three steps.

Step 1: To determine the optimal dimension of shorter slot (W_{s1}) to facilitate higher bandwidth over center frequency.
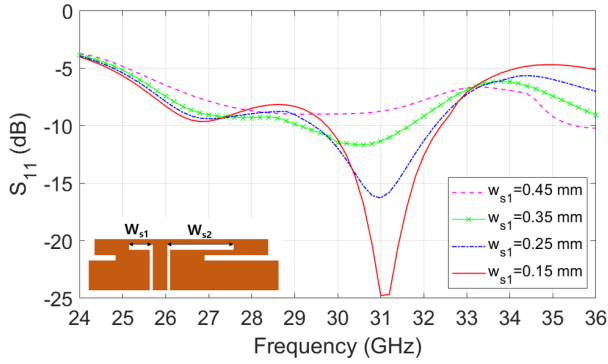
Fig. 6. Simulated reflection coefficient: effect of design parameter (W_{s1}) of the proposed antenna [see Fig. 2(a)] when $W_{s2} = 2.254$ mm.
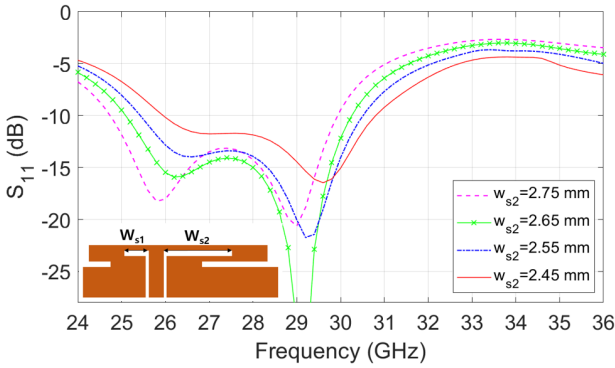

Fig. 7. Simulated reflection coefficient: effect of design parameter (W_{s2}) of the proposed antenna [see Fig. 2(a)] when $W_{s1} = 0.054$ mm.
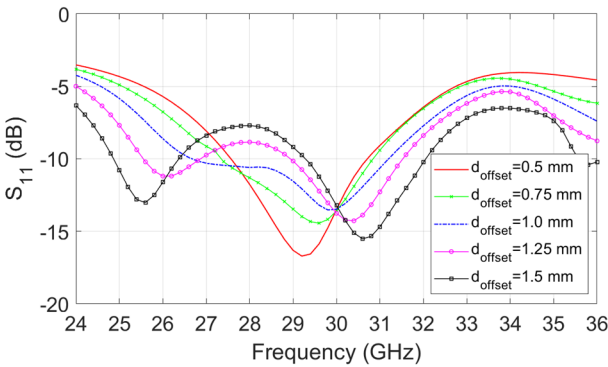

Fig. 8. Simulated reflection coefficient: effect of design parameter (d_{offset}) of the proposed antenna [see Fig. 2(a)].

Step 2: To determine the optimal dimension of longer slot (W_{s2}) to facilitate lower bandwidth under center frequency.

Step 3: Fine-tuning of degree of asymmetry parameter (d_{offset}) to improve impedance matching with the sum of slots ($W_{s1} + W_{s2}$) fixed.

An asymmetric topology is also advantageous in the main beam direction. Fig. 9(a) shows the *YZ* plane radiation pattern of the symmetric antenna. In this case, the current flows in two opposite directions along the antenna slots in the DS as shown in Fig. 10(a) such that the short dipoles for each slot radiate as a 1 × 2 array with an opposite phase. The main beam is divided in the broadside direction, with a null on the
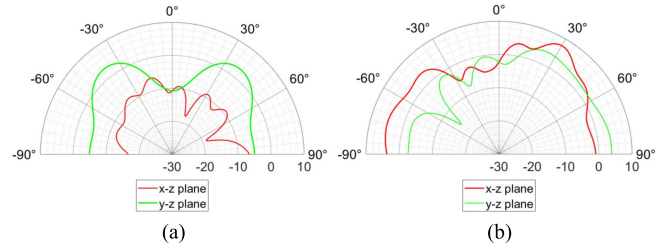

Fig. 9. Simulated radiation patterns: (a) symmetric slot antenna and (b) asymmetric folded dipole antenna with a CDGS. H-plane (red) and E-plane (green) at 28 GHz.
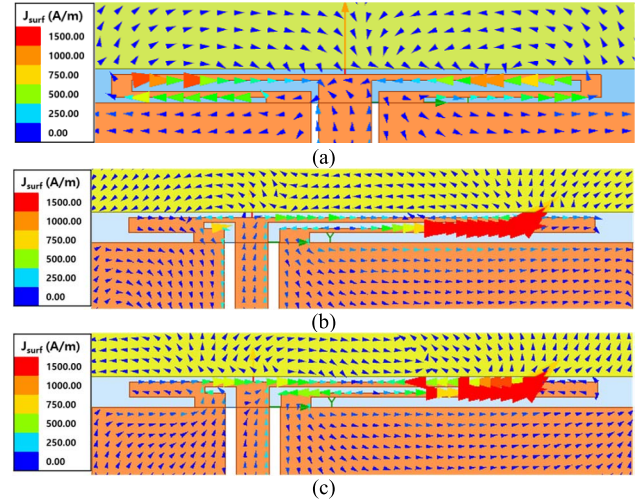

Fig. 10. Simulated surface current vector distributions at resonant frequency: (a) symmetrical slot antenna at 28 GHz; asymmetric FDA at (b) 27.1 GHz and (c) 29.3 GHz.

z-direction. On the other hand, Fig. 9(b) shows that proper optimization of the dimensions of the asymmetric features of the antenna can achieve the main beam near the broadside direction because the current directions are rendered along one direction from the two arms, as shown in Fig. 10(b) and (c). Fig. 10(b) shows that vector surface current is strongly distributed along the longer arm of the FDA at the lower frequency of operating bandwidth, and Fig. 10(c) shows that surface current vector is strongly distributed along the shorter arm as well as the longer arm at the higher frequency. Therefore, it was concluded that the proposed antenna is an asymmetric folded dipole antenna without a balun structure in the DS.

C. Superstrate Effect of Display Dielectric Layers

Several dielectric layers loaded over the antenna for the actual smartphone display configuration can constructively enhance the gain, as the proposed antenna layer is implanted between the display layers. There are three dielectric layers loaded on the antenna, which are the polarizer (Pol.), OCAs, and cover window. The Pol. is with thickness of 104 μm, and the relative constant of $\varepsilon_{r,pol.} = 2.92$. The OCA is with thickness of 150 μm, and dielectric constant of $\varepsilon_{r,oca} = 2.58$. The cover window is a tempered glass with the thickness of 480 μm and the dielectric constant of 6.9. Fig. 11 shows

TABLE I

DIMENSIONS OF THE PROPOSED ANTENNAS
(DIMENSIONS IN MILLIMETERS)

Designed Parameter	Dimension in Fig.2(a)	Description
d_{offset}	W_{s2} - W_{s1}	Degree of asymmetry
g	0.11	Gap of Coplanar waveguide
g_{ant}	0.1	Gap between antenna and the edge of CPW ground
g_{TS}	0.05	Gap between antenna and conductive panel
h_{COP}	0.1	Thickness of antenna film
L_{slot}	0.06	Length of slot
L_{ant}	0.15	Length of antenna
W_{a1}	1.225	Shorter width of antenna
W_{a2}	3.425	Longer width of antenna
W_{s1}	0.4765	Shorter width of slot
W_{s2}	2.6765	Longer width of slot
W_f	0.33	Signal line for impedance matching
W_{gnd}	5.2	Width of CPW ground
W_{dg}	0.4	Width of CDGS
t	0.0005	Metal thickness of antenna

* The optimal dimensions are chosen based on simulation, and resolution of fabrication reaches 1 μm.

that these dielectric superstrates can enhance the gain of the proposed antenna at the first resonant frequency by enhancing the electric distribution within the cover window. Finally, for design optimization, the width of the coplanar defected CPW ground and the different widths of the two slots inside the proposed antenna are the key parameters for impedance matching and broadside radiation pattern, and the dielectric superstrates rendered by display dielectric layers can enhance the gain of the proposed antenna topology. Extensive full-wave simulations were performed using ANSYS HFSS to optimize the impedance bandwidth and radiation efficiency while maintaining a near-broadside-directed main beam. The parameter dimensions of the proposed antenna are listed in Table I.

III. ANTENNA PERFORMANCE: SIMULATION AND RESULTS

To demonstrate the actual integration scenario in which the antenna is integrated at the edge of the smartphone display, the COP film as a substrate of the proposed CPW-fed asymmetric folded dipole antenna had a size of 38.57 × 30 mm. The length of the feed line was 8.57 mm to probe the antenna by a CPW edge launch connector, and the remaining 30 mm of the COP film, including the length of antenna, is inserted in the DS and AA areas. Each time the layers were stacked in order, the samples were strongly pressed by rolling a hard stick. By applying pressure, air bubbles between the floors were prevented, and the overall thickness was maintained uniformly. In this experimental prototyping, it is difficult to secure alignment accuracy between the folded dipole antenna and DS as well as the alignment accuracy between the display panels and the cover layers because the assembly process relies mostly on manual work while looking at the microscope. Fig. 12(a) shows the measurement setup for the proposed antenna mounted with a jig made of foam material, and Fig. 12(b) shows the fabricated sample of the proposed antenna. The input
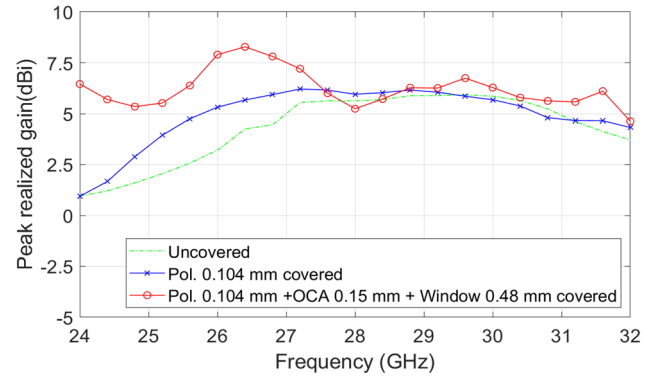

Fig. 11.   Simulated gain of the dielectric-loaded AiD.
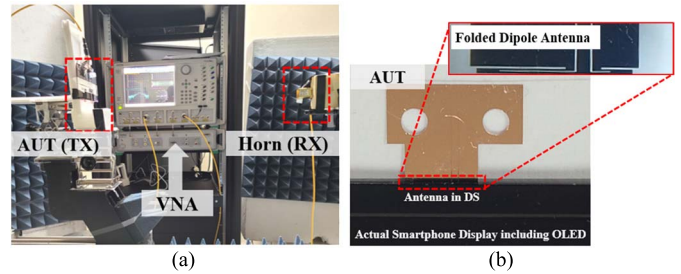

Fig. 12.   (a) Measurement setup with a vector network analyzer and (b) fabricated single antenna.
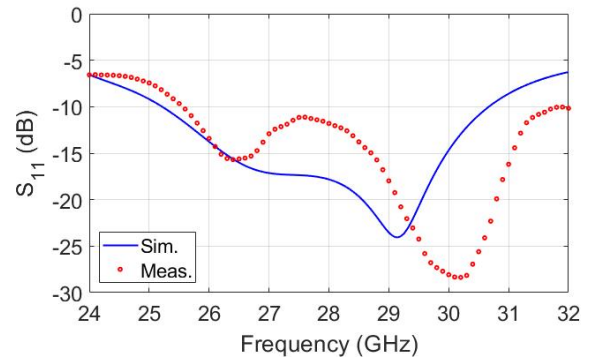
Fig. 13.   Measured and simulated S_{11} of the proposed antenna.

reflection coefficient $|S_{11}|$ of the proposed antenna is shown in Fig. 13 indicating the measured bandwidth of 6.3 GHz (25.6–31.9 GHz) and the simulated bandwidth of 5.3 GHz (25.3–30.6 GHz) where $|S_{11}| < -10$ dB. As expected, the divided resonance frequencies were observed through circuit analysis and simulation. It was found that shifts in the resonant frequencies occurred because a super-thin film had difficulties in accurately probing when the film was connected to the CPW edge launch connector. Furthermore, the misalignment between the display layers and the antenna due to the manual assembly process might have slightly changed the effective permittivity and, hence, the impedance matching.

The far-field radiation patterns of the fabricated antennas were measured in a millimeter-wave anechoic chamber at Seoul National University, Seoul, South Korea. The revolving arm with the antenna under test (AUT) was rotated in the hemisphere range, and the gain was measured by a standard

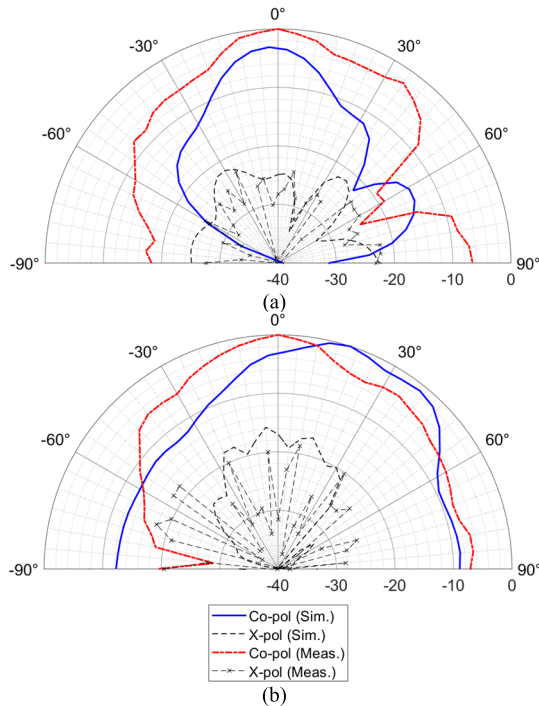Fig. 14. Measured and simulated results of normalized radiation pattern of a single element antenna in (a) E-plane and (b) H-plane. The operating frequency was measured and simulated at 28 GHz.

COMPARISON OF Tx–Rx MUTUAL CAPACITANCE CHANGE RATION BETWEEN CONVENTIONAL MESH-GRID PATCH AND THE PROPOSED AiD

Type	C_m	ΔC_m
Mesh-grid Patch	-26.1	-19.7
AiD in the DS	-32.1	-2.4

Fig. 15. Fabricated antenna sample by array elements without upper-than-antenna layers.

gain horn antenna (A-INFO 22-32). The range of the measured E-plane (*YZ* plane) and H-plane (*XZ* plane) of the proposed antenna was limited to the extent of interest because radiating the rear direction of a smartphone display was irrelevant. The peak gain of 7.85 dBi at 27.35 GHz and a 3 dB gain bandwidth of 1.45 GHz (25.95–27.4 GHz) were measured.

The measured and simulated normalized radiation patterns of the prototype are shown in Fig. 14. The co- and cross-polarized radiation intensity differences were at least more than 10 dB in all directions of interest in the E- and H-planes. The radiation pattern is slightly oriented toward the shorter slot of the antenna as expected, and the measured pattern of the H-plane is sharper and soared up. The difference in the far-field radiation patterns may potentially occur from the assembly process, in which the display panel pressure may cause a difference in the thickness of the COP film between the well-compressed antenna area and the uncompressed CPW line area.

The touch sensor performance is tested with a heat map of the mutual capacitance change ratio of the 32 × 16 unit cells at Samsung Display Company Ltd. First, the aggregate mutual capacitance (C_m) was measured without touching, and then, the change of the aggregate mutual capacitance (ΔC_m) was measured when the unit cell was touched. With a proper value of ΔC_m, the touch sensor could sense the touch, but when ΔC_m was reduced, there was a risk of malfunctioning of the touch sensor. For a reasonable comparison, mesh-grid patches were manufactured and integrated with the display as a reference to the existing studies. The size of a mesh-grid unit cell was set as 100 × 100 μm with a linewidth of 3 μm, and the patch size was set to be 3 × 3 mm. The value of C_m
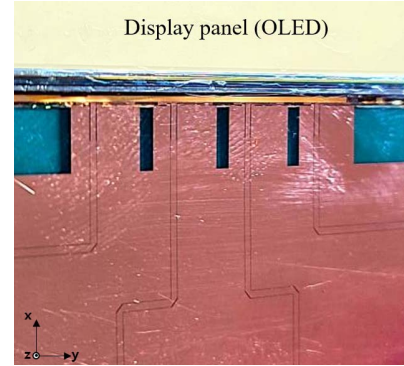
without any touch is decreased by −26.1% for the mesh-grid patch and −32.1% for the proposed AiD, due to the film attached on the touch sensor panel, as shown in Table II. The measured ΔC_m by touching the screen decreased by −19.7% for a mesh-grid patterned patch and −2.4% for the AiD. This successfully validates that the AiD has less effect on the TSP function. Furthermore, the standard draw test on the touchscreen worked normally.

IV. ARRAY FABRICATION AND MEASUREMENT

A. Design of the 1 × 4 Antenna Array

Based on the discussion in the previous sections, a 1 × 4 linear antenna array is designed for verification of beam scanning ability in the quad-channel beamforming system and fabricated on the COP film and affixed to the display panel in the same way as a single-element prototype. The fabricated sample is shown in Fig. 15. Because the higher insertion loss at 28 GHz along the CPW signal line is longer than the single-element sample, the insertion loss must be compensated for the accurate analysis of the fabricated array sample. In this case, a commonly used power divider is inappropriate for feed network. This is because the outer and inner antennas of the array receive unequal power but simultaneously radiate, making it impossible to compensate for the insertion loss of individual antenna elements. Furthermore, the discontinuities of the power divider close to the antenna elements also radiate. These unwanted radiating sources slightly distort the radiation pattern and affect the impedance matching. Therefore, the feed network of the array was chosen to be composed of four separate signal lines independently connected to the corresponding antenna element.
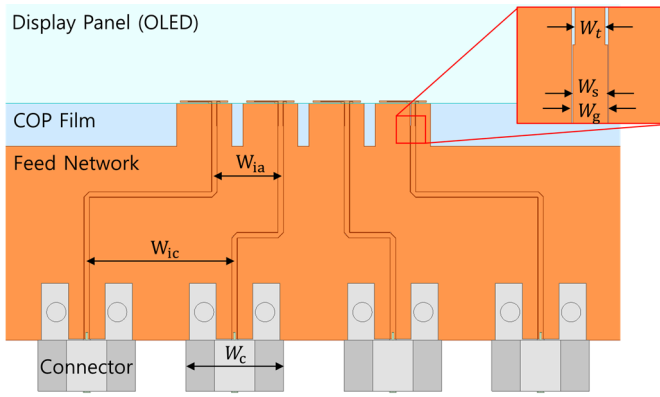
Fig. 16. Designed array feed network with dimension information ($W_t = 0.445$ mm, $W_s = 0.517$ mm, $W_g = 0.55$ mm, $W_{ia} = 6.5$ mm, and $W_{ic} = 9.5$ mm).
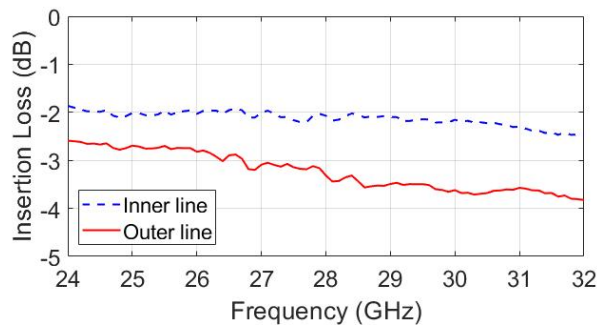

Fig. 18. Measured and simulated reflection coefficients of the outer and the inner antenna elements of the 1×4 antenna array sample.

Fig. 17. Measured insertion loss of inner and outer feed lines.

Fig. 19. Measured and simulated peak gain of the 1×4 antenna array sample.

The width of the connector was 10 mm, which was longer than the antenna array distance of 6.5 mm. Therefore, the four signal lines of the feed network had to be widened at the edge of the film to ensure that the edge launch connectors were affixed. By symmetry, the outer lines have the same length as the inner lines. However, the outer lines have different lengths from the inner lines because they are wider. For ease of measurement, the inner and outer lines were designed to have a $\lambda_{eff}/2$ difference in length such that each antenna was excited with the same phase. The insertion loss, including the transition losses between feed network and connector, was measured by the VNA, using the eight-port mirror-duplicated sample of the array feed network shown in Fig. 16. The measured insertion loss for the inner and outer feed lines is -1.97 and -3.05 dB (0.087 and 0.100 dB/mm) at the measured peak gain frequency of 27.1 GHz, as shown in Fig. 17. Because of the 1.08 dB difference in the insertion loss, the proposed four-line feed network may seem inferior to a power divider, and however, a power divider also has the same drawback because the outer and inner lines have different environments. Furthermore, the difference in the insertion losses incurred for each port in the proposed four-line feed network is not a problem because they are individually calibrated in the array pattern synthesis process, as described in the next paragraph.

B. 1 × 4 Antenna Array Measurement

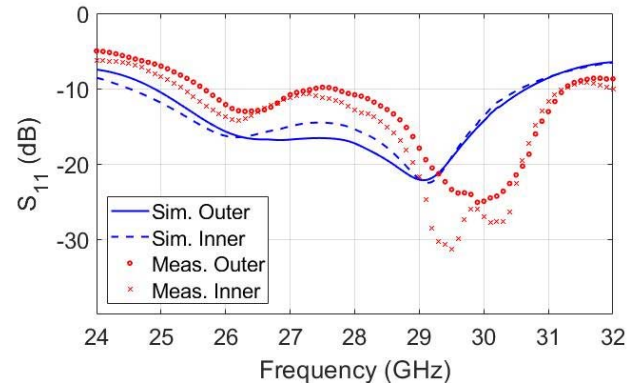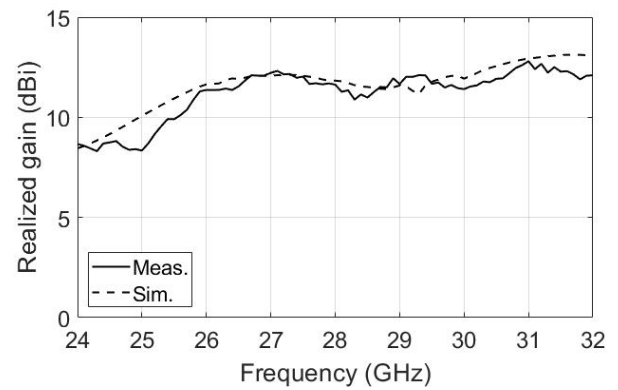The array gain is calculated from the individual measurement dataset at the four ports after insertion loss

compensation, using the active element pattern (AEP) technique [41]. To adopt the AEP technique, the gain pattern of each antenna element is measured, whereas the other three ports are terminated by 50 Ω loads. This technique accounts for the mutual coupling between array components, such as each element, CPW signal lines, and ground. Therefore, the array gain calculated from the AEP technique after antenna element measurement is identical to the gain directly measured using an ideal beamforming device.

The simulated and measured input reflection coefficients for the outer and inner elements of the antenna array are shown in Fig. 18. The measured and simulated impedance bandwidths of the outer elements of the antenna array were 5.6 GHz (25.6–31.2 GHz) and 5.8 GHz (24.9–30.7 GHz), respectively. Moreover, those of the inner elements of the antenna array were 5.9 GHz (25.3–31.2 GHz) and 6.1 GHz (24.5–30.6 GHz), respectively. The higher resonant frequency is shifted more than the lower resonant frequency of the single antenna. The slight discrepancy between the simulated and measured results is attributed to the same reason as that explained in Section III. Fig. 19 shows the simulated and measured array peak gains over frequency, which are in good agreement, proving the legitimacy of the AEP technique. The measured and simulated peak gains are 12.32, 11.63, and 12.12 dBi at 27.1, 28, and 27.2 GHz, respectively, in mm-Wave 5G frequency bands
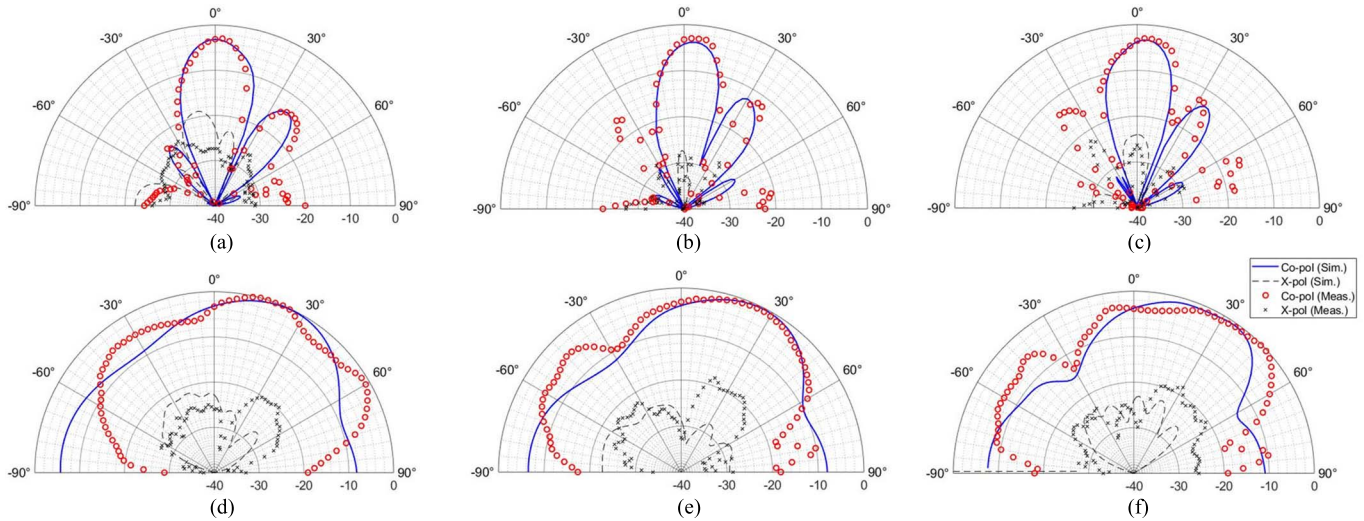
Fig. 20. Measured and simulated normalized far-field radiation patterns of the 1 × 4 antenna array sample in the E-plane at (a) 27.1 GHz, (b) 28 GHz, and (c) 29.3 GHz, and in the H-plane at (d) 27.1 GHz, (e) 28 GHz, and (f) 29.3 GHz.

TABLE III
SUMMARIZED FAR-FIELD RADIATION PERFORMANCE

Frequency (GHz)	Simulated Directivity (dBi)	Measured gain (dBi)	Efficiency (%)
27.1	14.97	12.32	54.33
28.0	14.63	11.63	50.12
29.3	14.24	12.11	61.24

around 28 GHz (n257, n258, and n261; 24.25–29.5 GHz). The simulated and measured 3 dB gain bandwidth covers 24.5–29.5 GHz and 25.3–29.5 GHz, most of the n257, n258, and n261 bands. The measured 3 dB gain bandwidth was wider than that of a single antenna element, suggesting the advantage of the phased-array configuration utilizing interelement effects. The radiation efficiency was 54.3%, which is comparable to the conventional results. The simulated and measured far-field radiation performances are presented in Table III.

The simulated and measured normalized far-field radiation patterns in the E- and H-plane are in good agreement with each other, at 27.1, 28, and 29.3 GHz, as shown in Fig. 20. Although the measured cross-polarization level is comparable with the measured co-polarization level in some directions in E-plane, this array design is acceptable because the co- and cross-polarized radiation level difference is greater than 10 dB for main beam direction at both of the resonant frequencies. Comparing Figs. 14 and 20, the difference between the simulated and measured radiation patterns is larger for single antenna element than antenna arrays. This is because a single antenna sample is much smaller than an array sample, making manual fabrication more difficult. The misalignment of the antenna and the DS changes the antenna operations of impedance matching and radiation efficiency. The scanning ability of the fabricated array samples was tested using the AEP technique once more. When the measured gain patterns of the single antenna elements were synthesized by the AEP technique,
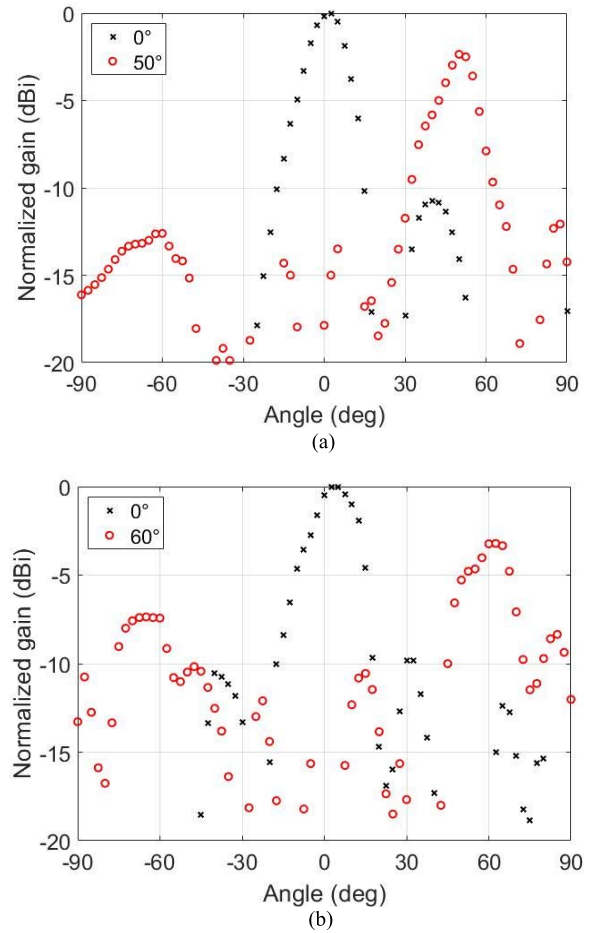

Fig. 21. Measured scanned far-field radiation patterns of the 1 × 4 array antenna sample in the E-plane at (a) 27.1 GHz and (b) 29.3 GHz.

phase shifts required for beam scanning were simply applied hypothetically, and the results are shown in Fig. 21. The antenna array sample proved a scanning ability of 50° and 60°

TABLE IV

COMPARISON OF THE PROPOSED AiD WITH OTHER DISPLAY-INTEGRATED ANTENNAS

Ref.	[17]	[18]	[20]	[23]	[30]	This work
Center frequency (GHz)	28	28	4.7 / 26 / 28	2.4	2.45	28
Material	Ag-alloy	Cu mesh-grid	Ni mesh-grid	Metal mesh-grid	Cu mesh-grid	Solid Cu
The ratio of material thickness to skin depth (%)	33	256	500	10.4	60.5	128
Effective conductivity (S/m)	2.5×10^7	N.A.	2×10^6	0.28×10^6	1.5×10^6	5.8×10^7
Antenna type	Patch	Patch	Patch	Patch	Patch	Folded-dipole
Antenna location	AA	AA	AA	AA	AA	DS
*Invisibility (%)	88	96	86	90	83	100
Radiation efficiency	41	N.A.	61	22	57	54.3
Gain (dBi)	9.16 / 6.66 (1 × 8 array)	1.7 (single)	9.6 (1 × 8 array)	-1.36 (single)	4.14 (single)	12.32 (1 × 4 array)
Flexibility	No	No	Yes	No	No	Yes

*Invisibility means optical transparency in other references.

at 27.1 and 29.3 GHz, respectively, within 5 dB of the possible scan loss.

The performance comparison between this study and previous studies on display antennas is summarized in Table IV. For an accurate characterization of the 1 × 4 array performance, four separate signal lines were used as a feed network and the AEP technique was applied to measure the gain and other properties. In the design step, unique techniques were used to significantly increase the gain of the antenna array. It should be noted that the proposed AiD is integrated with the display, as in previous studies, but is especially integrated with the narrow DS existing on the edge of the display panel, making it completely invisible to the user.

V. CONCLUSION

As an advanced display antenna research, this article presented and verified the concept of high-gain AiD for mm-wave 5G smartphone applications. The antenna located in the nonoptical DS of the display panel has many advantages over conventional display antennas designed on the AA of the display: better display visibility, touch sensor compatibility, low profile, and cost reduction. Above all, the proposed antenna could achieve high gain and high radiation efficiency using a highly conductive metal, whereas the conventional display antennas were made up of high resistive mesh-grid metal structure or transparent metal (e.g., ITO). Extensive analysis of the design parameters and measurements confirms that the narrow DS at the edge of the display panel is applicable for the high-gain 5G mm-wave display antenna design, suggesting the effectiveness of the proposed AiD concept. To prove the proposed AiD concept, a single element and a 1 × 4 linear antenna array were fabricated and successfully measured.

ACKNOWLEDGMENT

The authors would like to thank Hogyeom Kim, Fellow Researcher, for helping our measurement activities.

REFERENCES

[1] NR; User Equipment (UE) Radio Transmission and Reception; Part 2: Range 2 Standalone, Standard TS 38.101-2, v17.3.0, 3GPP, Sep. 2021.
[2] Y. P. Zhang and D. Liu, "Antenna-on-chip and antenna-in-package solutions to highly integrated millimeter-wave devices for wireless communications," IEEE Trans. Antennas Propag., vol. 57, no. 10, pp. 2830–2841, Oct. 2009.
[3] Z. Chen, Q. Liu, B. Smolders, P. Baltus, and H. Gao, "30-GHz co-designed low-noise amplifier and antenna-on-chip for wireless applications," in Proc. IEEE Int. Symp. Radio-Frequency Integr. Technol. (RFIT), Aug. 2019, pp. 1–3.
[4] K. S. Sultan, H. H. Abdullah, E. A. Abdallah, M. A. Basha, and H. H. El-Hennawy, "A 60-GHz gain enhanced vivaldi antenna on-chip," in Proc. IEEE Int. Symp. Antennas Propag. USNC/URSI Nat. Radio Sci. Meeting, Jul. 2018, pp. 1821–1822.
[5] Y. Ye, X. Zhao, and J. Wang, "Compact high-isolated MIMO antenna module with chip capacitive decoupler for 5G mobile terminals," IEEE Antennas Wireless Propag. Lett., vol. 21, no. 5, pp. 928–932, May 2022.
[6] H. Zhang and A. Shamim, "Gain enhancement of millimeter-wave on-chip antenna through an additively manufactured functional package," IEEE Trans. Antennas Propag., vol. 68, no. 6, pp. 4344–4353, Jun. 2020.
[7] Q. Liu, A. J. van den Biggelaar, U. Johannsen, M. C. van Beurden, and A. B. Smolders, "On-chip metal tiling for improving grounded mm-wave antenna-on-chip performance in standard low-cost packaging," IEEE Trans. Antennas Propag., vol. 68, no. 4, pp. 2638–2645, Apr. 2020.
[8] J. Choi et al., "Frequency-adjustable planar folded slot antenna using fully integrated multithrow function for 5G mobile devices at millimeter-wave spectrum," IEEE Trans. Microw. Theory Techn., vol. 68, no. 5, pp. 1872–1881, May 2020.
[9] H.-T. Chou and Z.-H. Lin, "Polarization agile beam steering by sub-array antenna module design to compensate wide-angle polarization discrepancy of user equipment antenna radiations at mmW frequencies," IEEE Trans. Antennas Propag., vol. 70, no. 9, pp. 8137–8147, Sep. 2022.
[10] L. Chi, Z. Weng, Y. Qi, and J. L. Drewniak, "A 60 GHz PCB wideband antenna-in-package for 5G/6G applications," IEEE Antennas Wireless Propag. Lett., vol. 19, no. 11, pp. 1968–1972, Nov. 2020.
[11] H.-C. Huang et al., "Miniaturized 5G module of wideband dual-polarized mm-wave antennas-in-package as non-mm-wave antennas (AiPaA) for handsets," in Proc. 16th Eur. Conf. Antennas Propag. (EuCAP), Mar. 2022, pp. 1–5.
[12] B. Yu et al., "A wideband mmWave antenna in fan-out wafer level packaging with tall vertical interconnects for 5G wireless communication," IEEE Trans. Antennas Propag., vol. 69, no. 10, pp. 6906–6911, Oct. 2021.

[13] J. Choi, D. Choi, J. Lee, W. Hwang, and W. Hong, "Adaptive 5G architecture for an mmWave antenna front-end package consisting of tunable matching network and surface-mount technology," *IEEE Trans. Compon., Packag., Manuf. Technol.*, vol. 10, no. 12, pp. 2037–2046, Dec. 2020.

[14] M. Xue, W. Wan, Q. Wang, and L. Cao, "Low-profile wideband millimeter-wave antenna-in-package suitable for embedded organic substrate package," *IEEE Trans. Antennas Propag.*, vol. 69, no. 8, pp. 4401–4411, Aug. 2021.

[15] J. Seo et al., "Miniaturized dual-band broadside/endfire antenna-in-package for 5G smartphone," *IEEE Trans. Antennas Propag.*, vol. 69, no. 12, pp. 8100–8114, Dec. 2021.

[16] R. Rodríguez-Cano, S. Zhang, and G. F. Pedersen, "Transparent mm-wave array on a glass substrate with surface wave reduction," in *Proc. 14th Eur. Conf. Antennas Propag. (EuCAP)*, Jul. 2020, pp. 1–4.

[17] J. Park, S. Y. Lee, J. Kim, D. Park, W. Choi, and W. Hong, "An optically invisible antenna-on-display concept for millimeter-wave 5G cellular devices," *IEEE Trans. Antennas Propag.*, vol. 67, no. 5, pp. 2942–2952, May 2019.

[18] J. M. Heo, E. J. Sung, J. K. Kim, and G. Byun, "Character-istic impedance adjustment of thin-metal mesh transmission lines for mmWave display-integrated antennas," *IEEE Access*, vol. 9, pp. 94714–94722, 2021.

[19] J. Park et al., "Circuit-on-display: A flexible, invisible hybrid electro-magnetic sensor concept," *IEEE J. Microw.*, vol. 1, no. 2, pp. 550–559, Apr. 2021.

[20] H. C. Qiu et al., "Compact, flexible, and transparent antennas based on embedded metallic mesh for wearable devices in 5G wireless network," *IEEE Trans. Antennas Propag.*, vol. 69, no. 4, pp. 1864–1873, Apr. 2021.

[21] W. Hong, K.-H. Baek, and S. Ko, "Millimeter-wave 5G antennas for smartphones: Overview and experimental demonstration," *IEEE Trans. Antennas Propag.*, vol. 65, no. 12, pp. 6250–6261, Dec. 2017.

[22] J. Park et al., "OLED display-integrated optically invisible phased arrays for millimeter-wave 5G cellular devices," in *IEEE MTT-S Int. Microw. Symp. Dig.*, pp. 699–702, Oct. 2020.

[23] W. Hong, S. Lim, S. Ko, and Y. G. Kim, "Optically invisible antenna integrated within an OLED touch display panel for IoT applica-tions," *IEEE Trans. Antennas Propag.*, vol. 65, no. 7, pp. 3750–3755, Jul. 2017.

[24] S. Foo and W. Tong, "AMOLED in-display antennas," in *Proc. 14th Eur. Conf. Antennas Propag. (EuCAP)*, Mar. 2020, pp. 1–5.

[25] Z. Yong, "A transparent dual-band dual-polarized mm-wave antenna array for 5G smartphone application," in *Proc. Int. Symp. Antennas Propag. (ISAP)*, Oct. 2019, pp. 1–3.

[26] R. H. Mohammad, N. M. Mohammad, A. L. N. Abbas, and N. Alireza, "Improving the efficiency of transparent antenna using gold nanolayer deposition," *IEEE Antennas Wireless Propag. Lett.*, vol. 15, pp. 4–7, 2016.

[27] P. Duy Tung and C. W. Jung, "Optically transparent wideband dipole and patch external antennas using metal mesh for UHD TV applica-tions," *IEEE Trans. Antennas Propag.*, vol. 68, no. 3, pp. 1907–1917, Mar. 2020.

[28] S. Hong, S. H. Kang, Y. Kim, and C. W. Jung, "Transparent and flex-ible antenna for wearable glasses applications," *IEEE Trans. Antennas Propag.*, vol. 64, no. 7, pp. 2797–2804, Jul. 2016.

[29] S. Hong, Y. Kim, and C. W. Jung, "Transparent microstrip patch antennas with multilayer and metal-mesh films," *IEEE Antennas Wireless Propag. Lett.*, vol. 16, pp. 772–775, 2017.

[30] S. H. Kang and C. W. Jung, "Transparent patch antenna using metal mesh," *IEEE Trans. Antennas Propag.*, vol. 66, no. 4, pp. 2095–2100, Apr. 2018.

[31] S. Morris, A. R. Chandran, N. Timmons, and J. Morrison, "The fab-rication and analysis of a polyimide based loop antenna for 2.45 GHz WBAN applications," in *Proc. Loughborough Antennas Propag. Conf. (LAPC)*, Nov. 2016, pp. 1–4.

[32] H. R. Khaleel, H. M. Al-Rizzo, and D. G. Rucker, "Compact polyimide-based antennas for flexible displays," *J. Display Technol.*, vol. 8, no. 2, pp. 91–97, Feb. 2012.

[33] S.-C. Chiu and S.-Y. Chen, "Miniaturization of CPW-fed slot antenna using a pair of interdigital capacitors," in *Proc. IEEE Antennas Propag. Soc. Int. Symp. (APSURSI)*, Jul. 2013, pp. 1380–1381.

[34] C.-C. Yu and X.-C. Lin, "A wideband single chip inductor-loaded CPW-fed inductive slot antenna," *IEEE Trans. Antennas Propag.*, vol. 56, no. 5, pp. 1498–1501, May 2008.

[35] N. Pazare, R. Kumar, R. V. S. R. Krishna, and K. Ramkrishnan, "Design of asymmetric CPW fed slot antennas for pattern and polarization diver-sity," in *Proc. IEEE Global Conf. Wireless Comput. Netw. (GCWCN)*, Dec. 2014, pp. 36–40.

[36] C. Peng, I. Chen, and J. Yeh, "Printed broadband asymmetric dual-loop antenna for WLAN/WiMAX applications," *IEEE Antennas Wireless Propag. Lett.*, vol. 12, pp. 898–901, 2013.

[37] K.-L. Wong and Y.-C. Chen, "Small-size hybrid loop/open-slot antenna for the LTE smartphone," *IEEE Trans. Antennas Propag.*, vol. 63, no. 12, pp. 5837–5841, Dec. 2015.

[38] W. A. Awan, S. I. Naqvi, A. H. Naqvi, S. M. Abbas, A. Zaidi, and N. Hussain, "Design and characterization of wideband printed antenna based on DGS for 28 GHz 5G applications," *J. Electromagn. Eng. Sci.*, vol. 21, no. 3, pp. 177–183, Jul. 2021.

[39] C. Ramakrishna, G. A. E. S. Kumar, and P. C. S. Reddy, "Quadruple band-notched compact monopole UWB antenna for wireless applica-tions," *J. Electromagn. Eng. Sci.*, vol. 21, no. 5, pp. 406–416, Nov. 2021.

[40] D. K. Kong, J. Kim, D. Woo, and Y. J. Yoon, "Broadband modified proximity coupled patch antenna with cavity-backed configuration," *J. Electromagn. Eng. Sci.*, vol. 21, no. 1, pp. 8–14, Jan. 2021.

[41] D. M. Pozar, "The active element pattern," *IEEE Trans. Antennas Propag.*, vol. 42, no. 8, pp. 1176–1178, Sep. 1994.

[42] T.-H. Chang and J.-F. Kiang, "Bandwidth broadening of dielectric resonator antenna by merging adjacent bands," *IEEE Trans. Antennas Propag.*, vol. 57, no. 10, pp. 3316–3320, Oct. 2009.

[43] A. A. Omar, J. Park, W. Kwon, and W. Hong, "A compact wide-band vertically polarized end-fire millimeter-wave antenna utilizing slot, dielectric, and cavity resonators," *IEEE Trans. Antennas Propag.*, vol. 69, no. 9, pp. 5234–5243, Sep. 2021.

[44] M. Chai, K. Parikh, B. D. Horine, T. A. Nugraha, K. H. Lee, and H. G. Skinner, "Display integrated antenna," U.S. Patent 14 751 707, Jun. 1, 2015.

[45] Z. Su, K. Klionovski, H. Liao, Y. Chen, A. Z. Elsherbeni, and A. Shamim, "Antenna-on-package design: Achieving near-isotropic radi-ation pattern and wide CP coverage simultaneously," *IEEE Trans. Antennas Propag.*, vol. 69, no. 7, pp. 3740–3749, Jul. 2021.

[46] M. Moallem et al., "High performance mm-wave MIMO radar with integrated antenna-on-package," in *Proc. IEEE 70th Electron. Compon. Technol. Conf. (ECTC)*, Jun. 2020, pp. 108–113.

[47] C.-Y. Ho, M.-F. Jhong, P.-C. Pan, C.-Y. Ting, and C.-C. Wang, "Antenna-on-package on low-cost organic substrate for 60 GHz wireless communi-cation applications," in *Proc. 18th Int. Conf. Electron. Packag. Technol. (ICEPT)*, Aug. 2017, pp. 192–196.

Jeongtaek Oh (Graduate Student Member, IEEE) received the B.S. degree in electrical and computer engineering from Seoul National University, Seoul, South Korea, in 2020, where he is currently pursuing the integrated master's and Ph.D. degrees.

His current research interests include display antennas and metamaterial-based transmitarray antennas for mmWave communication systems.

Byeongjin Kim (Graduate Student Member, IEEE) received the B.S. degree in electrical and computer engineering from Seoul National University, Seoul, South Korea, in 2020, where he is currently pursuing the integrated master's and Ph.D. degrees.

His current research interests include display ant-enna and transmitarray antenna for 5G millimeter-wave communication systems.

Sangrock Yoon (Member, IEEE) received the M.S. degree in information and communication engi-neering from Yeungnam University, Gyeongsan, South Korea, in 2001.

He is currently a Principal Engineer with Samsung Display Company Ltd., Kiheung, South Korea. His current research interests include optically transpar-ent display-integrated antennas for mmWave 5G/6G communication systems.

Kiseo Kim received the M.Sc. degree in physics from Kyung-Hee University, Seoul, South Korea, in 2008.

He is currently an Engineer with Samsung Display Company Ltd., Kiheung, South Korea. His research interests include display-integrated antennas and next-generation displays.

Jungsuek Oh (Senior Member, IEEE) received the B.S. and M.S. degrees from Seoul National University, Seoul, South Korea, in 2002 and 2007, respectively, and the Ph.D. degree from the University of Michigan, Ann Arbor, MI, USA, in 2012.

From 2007 to 2008, he was with Korea Telecom, Seongnam-si, South Korea, as a Hardware Research Engineer, working on the development of flexible RF devices. From 2013 to 2014, he was a Staff RF Engineer with Samsung Research America, Dallas, TX, USA, working as a Project Leader for the 5G/millimeter-wave antenna system. From 2015 to 2018, he was a Faculty Member at the Department of Electronic Engineering, Inha University, Incheon, South Korea. He is currently an Associate Professor with the Department of Electrical and Computer Engineering, Seoul National University. He has published more than 60 technical journals and conference papers. His research interests include mmWave metasurface/lens beam focusing/shaping techniques, antenna miniaturization for integrated systems, and radio propagation modeling for complex scenarios.

Prof. Oh was a recipient of the 2011 Rackham Predoctoral Fellowship Award at the University of Michigan. He has served as a Technical Reviewer for the IEEE TRANSACTIONS ON ANTENNAS AND PROPAGATION and IEEE ANTENNAS AND WIRELESS PROPAGATION LETTERS. He has served as a TPC Member and the Session Chair for numerous conferences, such as IEEE Antennas and Propagation Society (AP-S) and the US National Committee (USNC) of the International Union of Radio Science (URSI), the International Symposium on Antennas and Propagation (ISAP), and the Korean Institutes of Electromagnetic Engineering and Science (KIEE) conferences, where his team has been awarded honorably.

Eun Jin Sung (Member, IEEE) received the B.A. degree in computer science engineering from Dongguk University, Seoul, South Korea, in 2013.

Her current research interests include OLED panel architecture and module structure for display antennas.